Von P. Walden[1]*, Stephen G. Warren[2], and Elizabeth Tuttle[3]

[1]University of Idaho, [2]University of Washington, and [3]Antioch University

## 1. INTRODUCTION

Ice crystals are nearly always present in the atmospheric boundary layer over the Antarctic Plateau. They interact with both solar and infrared radiation and therefore affect the planetary energy budget. Regional models and general-circulation models are sensitive to the shapes and sizes of ice crystals and water droplets specified for antarctic clouds (Lubin et al. 1998).

It has been difficult to retrieve properties of clouds over snow using satellite instruments, such as the Advanced Very High Resolution Radiometer (AVHRR). With new instruments becoming available, such as the Moderate-resolution Infrared Spectrometer (MODIS) and the Atmospheric Infrared Sounder (AIRS), more information should be retrievable, and it will be essential to have in-situ data with which to evaluate the retrievals.

Previous studies on Antarctic summertime ice crystal precipitation include Hogan (1975), Kikuchi and Hogan (1979), Ohtake (1978), and Tape (1994). Ohtake and Yogi (1979) reported on ice crystals observed in the antarctic winter.

Throughout the six-month winter (April-September) on the Antarctic Plateau, a strong surface-based temperature inversion persists. Vertical mixing within this layer, which may be facilitated by horizontal winds flowing over the rough snow surface, causes the boundary-layer air to become supersaturated with respect to ice, so small ice crystals, called "diamond dust", form in the inversion layer. Longwave cooling of the near-surface air can also lead to supersaturation and ice-crystal formation, even in the absence of mixing. Longwave radiation from clouds aloft can weaken the inversion, but cannot destroy it completely, so diamond dust often forms even under clouds.

Based on visual observations made by the South Pole Weather Office in six different years, ice crystals have been observed to be absent in the near-surface atmosphere about 9% of the time in winter. In contrast, diamond dust is reported about 63% of the time, and blowing snow about 39%.

_____

*  *Corresponding author address*:  Von P. Walden, University of Idaho, Department of Geography, Moscow, Idaho 83844-3021;
email: vonw@uidaho.edu.

Since they are both quite common and often occur together, the sum of their frequencies of occurrence may exceed 100%. Larger snow grains, falling from clouds, are reported much less often (7%), but non-precipitating clouds are common.

Here we present information on the shapes and sizes of wintertime ice crystals over South Pole Station. The effective radii for the three major types of ice crystals, diamond-dust, blowing snow, and snow grains, are presented and discussed. This extended abstract is an excerpt from a longer manuscript by Walden et al. (2003).

## 2. OBSERVATIONS AND METHODS

### 2.1 Photomicrographs of Ice Crystals

From 28 June to 30 September 1992, a gridded microscope slide was placed on an elevated platform on the roof of the Clean Air Facility at South Pole Station and allowed to collect ice crystals. The ice crystals fell naturally onto the uncoated slide, which was scribed with minor grid lines with spacings of 50 μm. The average collection time was about 3 hours, but ranged from 30 minutes to 6 hours. Calculations of terminal velocities show that the slide was exposed long enough to adequately sample the various types of falling crystals. Due to the low values of the minimum concentration necessary to sample the various crystal types, we probably did not miss any significant types of crystals.

After exposure to the atmosphere, the slide was taken to an unheated vestibule where the microscope was kept; the temperature of the microscope was typically –40°C. A Nikon F3 camera with Kodak TMAX 100 black-and-white film was attached to the microscope to photograph the gridded slide.

For this study, we used 84 images, and measured over 20,000 ice crystals. The images represent an adequate sample of wintertime ice crystals over the Antarctic Plateau, since they were obtained under all types of meteorological conditions throughout the winter. The ice crystals were collected at surface air temperatures ranging from -73°C to -35°C. For these months, meteorological data are available from the South Pole Weather Office, including surface measurements of temperature, pressure, wind speed and direction, visual surface observations of sky

conditions, and temperature profiles from daily radiosondes.

The photographs were digitized using an electronic scanner at 300 dots per inch (dpi) and were stored as TIFF (tagged image format file) images. The images were displayed and sized using image-processing software. A scale factor (0.74 µm/pixel) was determined by drawing a vector between grid lines of known separation on the slide. The uncertainty in sizing ice crystals was estimated by repeatedly measuring the distance between various grid lines on a few representative images, and is about 1 µm for the range of sizes of interest, 1 to 1000 µm.

## 2.2 Classification of Ice-Crystal Shapes

Table 1 (on last page) shows the nine types of ice crystals identified in the images and the number of crystals that were sized of each type. Each crystal type requires at least one dimension for its description, but some require as many as three. These dimensions are illustrated in the sketches in Table 1. Bullet clusters have, in addition, a value $n$ that designates the number of crystals in the cluster. Table 2 (on last page) shows the relative frequency of occurrence of the different ice crystal types. Also shown in Table 2 are the relative contributions of each crystal type to the total surface area and total volume. All three quantities were obtained by dividing the number of crystals on each photomicrograph by the slide exposure time and also accounting for the different areas photographed depending on the magnification used.

The crystals can be separated into three major categories: diamond dust, blowing snow, and snow grains. Figure 1 shows an example of a photomicrograph that contains all three types of ice crystals; the grid lines on the microscope slide are visible in the image. The small, rounded crystals are blowing snow; the bullet clusters are snow grains; and there are both long and short columns of diamond dust.

Each crystal is classified into one of the three major categories based on its size and shape. Diamond dust and snow grains are distinguished from blowing snow by their shape; diamond dust and snow grains have crystalline shapes, while blowing snow are rounded particles. Diamond-dust crystals are distinguished from snow grains by size, primarily thickness.

## 2.3 Effective Radius

The crystal dimensions are used to calculate the surface area and volume for each crystal. The appropriate mensuration formulae are used for each crystal shape. The size distributions for each crystal type are generated by first representing the non-spherical ice particles by a collection of "equivalent" spheres, $r_{VA}$. Spheres with the same volume-to-area ratio ($V/A$) as the crystals are used here because of the importance of $V/A$ in calculating radiative fluxes and heating rates in atmospheric radiation models. Grenfell and Warren (1999) have shown that equal-V/A spheres provide a good approximation for the extinction efficiency, the single-scattering albedo, and the asymmetry parameter over a wide range of wavelengths from the ultraviolet through the infrared. A single non-spherical particle is represented by a collection of independent spheres that has the same total surface area and the same total volume as the nonspherical particle.
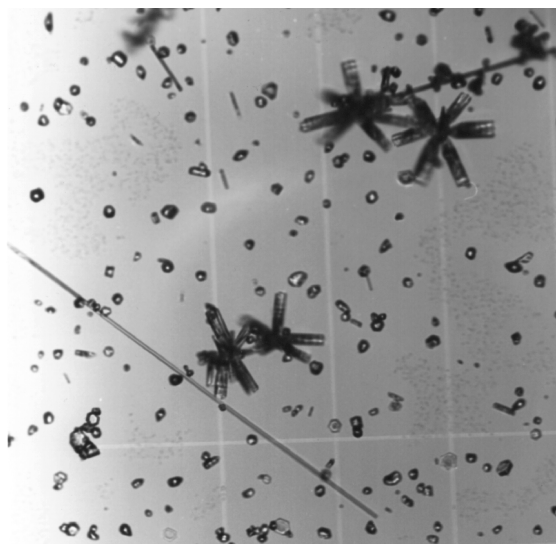


**Figure 1**. Photomicrographs of wintertime ice crystals at South Pole Station. This example shows a mixture of "long prism" diamond-dust crystals, small rounded blowing-snow particles, and small snow grains (bullet clusters). The image was taken on 14 July 1992. The major scribe lines are spaced 250 µm apart.

Some authors (e.g. Fu *et al.* 1999) prefer to use projected area $P$ instead of total surface area $A$ when computing the equivalent radius. For convex particles the two methods give exactly the same value of $r_{VA}$, because $A=4P$ for all convex shapes (Vouk 1948), so $r_{VA}=3V/A = 3V/4P$. However, for crystals with concavities, we think it is probably important to count the inner surfaces when using spheres to mimic such a crystal, since scattering can occur at those surfaces as well as at the external surfaces. For this reason we prefer to define equivalent radius in terms of total surface area instead of projected area, so that it can be applied to all nonspherical crystals, not just convex shapes.

Hexagonal plates often have unequal sides. We believe that this is probably true for columns as well, although this asymmetry was not measured. Since the

columns were assumed to have all sides equal, but were probably asymmetric and lying on their broad side, our estimates of the surface area and volume are both biased high. Laboratory experiments by Bailey and Hallett (2000) and Kajikawa et al. (1980) find that the width of the broad sides is typically 1.6-2.5 times the width of the narrow sides. These biases tend to cancel somewhat when calculating the V/A ratio, but $r_{VA}$ is still probably biased high by 15-50%.

For radiative transfer calculations, the most important single measure of a size distribution is the area-weighted mean radius, or "effective radius", $r_{eff}$, which was defined for spheres by Hansen and Travis (1974):

$$r_{eff} = \frac{\int r^3 n(r)\, dr}{\int r^2 n(r)\, dr} \quad . \qquad (3)$$

For each crystal, we compute the equivalent radius and its associated number of equivalent spheres, then we compute $r_{eff}$ for a size distribution for many ice crystals.

## 3. MEASUREMENTS OF CRYSTAL DIMENSIONS, SIZE DISTRIBUTIONS, AND EFFECTIVE RADII

Table 1 gives the means and extremes of the crystal dimensions. The longest dimension was 1000 μm, the c-axis of the long diamond-dust column in Figure 1. The smallest dimension was 2 μm, which occurred for solid columns. The smallest mean dimension was the width of solid columns and the thickness of plates, 13 μm; the largest mean was the c-axis of the bullets in bullet clusters, 243 μm.

Figure 2 displays the dimensions of diamond-dust ice crystals, plotted as the crystal length (c) versus crystal width (2a). By definition, columns have an aspect ratio greater than 1, while plates have $c/2a < 1$. Shimizu (1963) first demonstrated the existence of "long prisms", now sometimes called Shimizu crystals, for which $c/2a > 5$. Figure 2 shows that these crystals are quite common. The crystal with the maximum value of $c/2a$ (about 100) for the entire 1992 dataset is shown in Figure 1. The values of 2a for diamond dust range from 2 to 158 μm; the values of c range from 3 to 1000 μm.

Figure 2 shows a paucity of equidimensional crystals ($c \approx 2a$). This is not an artifact of the process of sizing the crystals due to the choice of whether a crystal is a column or a plate, or due to how the plates with one measurable dimension are handled. It is rather a real feature that suggests that diamond-dust crystals are rarely equidimensional.

Blowing-snow particles are small, with semi-dimensions between 1 and 65 μm (not shown). By definition, the semi-major axis a is longer than the semi-minor axis b. The average values of 2a and 2b are 19 μm and 15 μm. The average aspect ratio (a/b) is 1.4 for blowing snow.
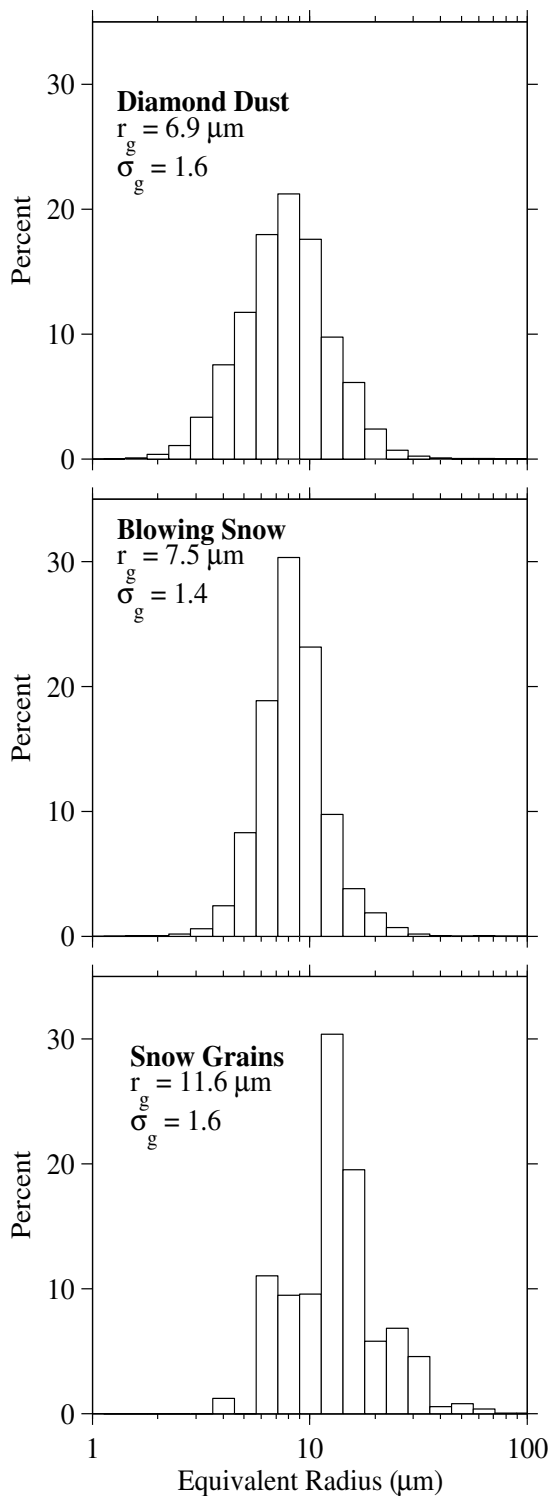
Figure 3 shows the size distributions of the three major categories of ice crystals. These figures are plotted on a semi-log graph because the size distributions resemble log-normal distributions (Reist 1993). The geometric mean radius ($r_g$) and geometric standard deviation ($\sigma_g$) are listed in Figure 3.

The effective radius $r_{eff}$ for diamond dust is 12.2 μm. This is a weighted average of columns ($r_{eff}$ = 10.1 μm) and plates ($r_{eff}$ = 15.1 μm). The effective radius for hollow columns ($r_{eff}$ = 6.4 μm) is much smaller than that for solid columns, but hollow columns are very rare. The effective radius for blowing snow is 11 μm. Snow grains are larger than both diamond dust and blowing snow, with an effective radius of 24 μm. Snow-grain columns are much larger ($r_{eff}$ = 67 μm) than both sector-plate clusters (12 μm) and bullet clusters (25 μm), because the sector-plates in clusters are thin (assumed 10 μm) and bullets are hollow.
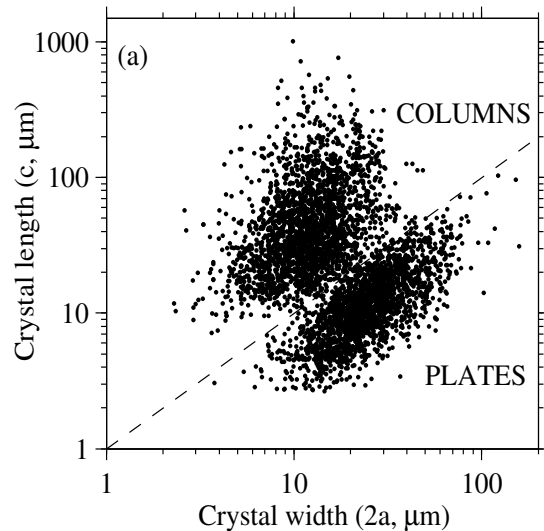


**Figure 2**. Dimensions of solid columns and plates. The dashed line with slope of 1 designates the boundary between plates ($c/2a \leq 1$) and columns ($c/2a > 1$). "Long prism" columns were defined by Shimizu (1963) as those having $c/2a > 5$. There are 4,495 crystals plotted here.

Figure 4 shows the distribution of daily effective radii for each of the 84 days that were sampled. The most probable effective radius is about 11 μm for any given day in this dataset; this is roughly the effective radius of blowing snow and diamond

**Figure 3**. Size distributions of the three main types of wintertime ice crystals. The geometric mean ($r_g$) and standard deviations ($\sigma_g$) are listed for each distribution. The histograms show the percent occurrence of equivalent spheres.

dust. There were a few days when larger particles dominated; the images for these days were largely populated with snow grains.
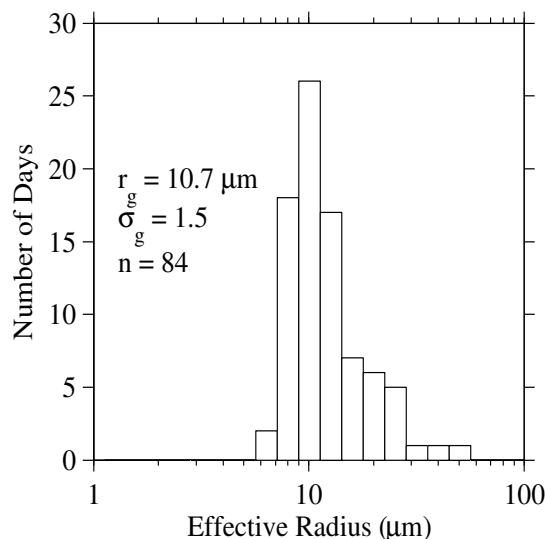


**Figure 4**. An effective radius was determined for the entire assemblage of crystals on each day. The frequency distribution of the daily effective radii is plotted here.

## 4. CORRELATION WITH METEOROLOGICAL CONDITIONS

Attempts were made to correlate the aspect ratio of diamond dust (*c/2a*) and the semi-major axis of blowing snow with meteorological conditions using surface meteorological measurements and radiosonde profiles from the South Pole Weather Office (SPWO). None of the correlations with diamond dust are significant. Although not significant, the data indicate a decrease in particle size of both diamond dust and blowing snow with increasing wind speed. The only significant correlation for the semi-major axis of blowing snow is with the inversion-top temperature ($r^2=0.31$), although there is no apparent reason for this. Because of the weak correlations, the size distributions presented here can be expected to represent conditions throughout the entire antarctic winter.

## 5. CONCLUSIONS

Nine different types of ice crystals were identified and sized for the antarctic winter of 1992. These crystals are categorized into three main groups: diamond dust, blowing snow, and snow grains. Wintertime diamond-dust ice crystals, which are primarily solid columns and plates, have a wide range of aspect ratios. Blowing-snow particles are small and round, with aspect ratios near 1. Snow grains, which

precipitate from clouds, have much larger surface area and volume than either diamond dust or blowing snow, but occur much less frequently. The effective radii for diamond dust, blowing snow, and snow grains are 12 µm, 11 µm, and 24 µm. Although diamond-dust particles are much longer than blowing-snow particles, their short dimensions are similar, and it is their short dimensions that primarily determine their equivalent radius.

The aspect ratio of diamond-dust ice crystals, and the size of blowing-snow particles, are uncorrelated with meteorological conditions measured at the surface or within the near-surface temperature inversion. This suggests that the size distributions presented here may be used to represent the entire antarctic winter. Size distributions are presented for the three main categories of crystals, along with the geometric mean radii and standard. The size distribution of effective radii for each day is presented. The most probable effective radius in wintertime is about 11 µm.

## 8. REFERENCES

Bailey, M. and J. Hallett, 2000: Nucleation, growth, and habit distribution of cirrus type crystals under controlled laboratory conditions. *13th International Conference on Clouds and Precipitation*, August 14-18, 2000, Reno, Nevada, 629-632.

Blanchet, J.-P., and E. Girard, 1994: Arctic greenhouse cooling, *Nature*, **371**, 383.

Fu, Q., W.B. Sun, and P. Yang, 1999: Modeling of scattering and absorption by nonspherical cirrus ice particles at thermal infrared wavelengths. *J. Atmos. Sci.,* **56**, 2937-2947.

Grenfell, T.C., and S.G. Warren, 1999: Representation of a nonspherical ice particle by a collection of independent spheres for scattering and absorption of radiation. *J. Geophys. Res.*, **104**, 31697-31709.

Hansen, J.E., and L.D. Travis, 1974: Light scattering in planetary atmospheres, *Space Sci. Rev*., **16**, 527-610.

Hogan, A.W., 1975: Summer ice crystal precipitation at the South Pole, *J. Appl. Meteor.*, **14**, 246-49.

Kajikawa, M., K. Kukuchi, and C. Magono, 1980: Frequency of occurrence of peculiar shapes of snow crystals. *J. Meteor. Soc. Japan*, **58**, 416-421.

Kikuchi, K., 1972: Sintering phenomenon of frozen cloud particles observed at Syowa Station, Antarctica, *J. Met. Soc. Japan*, **50**, 131-135.

Kikuchi, K., and A.W. Hogan, 1979: Properties of diamond dust type ice crystals observed in summer season at Amundsen-Scott South Pole Station, Antarctica, *J. Met. Soc. Japan*, **57**, 180-190.

Lubin, D., B. Chen, D.H. Bromwich, R.C.J. Somerville, W.-H. Lee, and K.M. Hines, 1998: The impact of antarctic cloud radiative properties on a GCM climate simulation, *J. Climate*, **11**, 447–462.

Ohtake, T., 1978: Atmospheric ice crystals at the South Pole in summer, *Antarctic J. U. S.*, **13**, 174-175.

Ohtake, T. and T. Yogi, 1979: Winter ice crystals at the South Pole. *Antarctic J. U. S.*, **14**, 201-203.

Reist, P. C., 1993: *Aerosol Science and Technology, 2nd edition*, McGraw-Hill, Inc., New York, 379 pp.

Shimizu, H., 1963: "Long prism" crystals observed in the precipitation in Antarctica. *J. Met. Soc. Japan*, **41**, 305-307.

Tape, W., 1994: *Atmospheric Halos*. Antarctic Research Series, volume 64, American Geophysical Union, Washington, D.C., 143 pp.

Vouk, V., 1948: Projected area of convex bodies. *Nature,* **162,** 330-331.

Walden, V.P., S.G. Warren, and E. Tuttle, 2003: Atmopsheric ice crystals over the Antarctic Plateau in winter, *J. Appl. Meteor.*, in review.

Table 1: Types of crystals that were identified and sized from the photomicrographs.
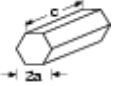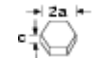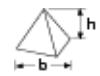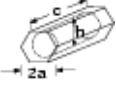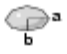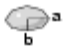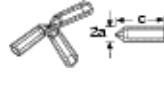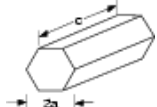
| Crystal Type | Number Sized | Shape | | Dimension (μm) | | |
|---|---|---|---|---|---|---|
| | | | | Min. | Max. | Mean |
| ***Diamond Dust*** | | | | | | |
| Solid Columns | 2381 | | 2a | 2 | 49 | 13 |
| | | | c | 7 | 1006 | 61 |
| Plates | 2127 | | 2a | 4 | 158 | 27 |
| | | | c | 3 | 103 | 13 |
| Pyramids | 95 | | b | 13 | 57 | 29 |
| | | | h | 9 | 48 | 22 |
| Hollow Columns | 21 | | 2a | 8 | 34 | 16 |
| | | | c | 31 | 208 | 85 |
| | | | h | 4 | 21 | 9 |
| ***Blowing Snow*** | | | | | | |
| Blowing Snow | 12,958 | | 2a | 4 | 130 | 19 |
| | | | 2b | 3 | 97 | 15 |
| Residual Blowing Snow | 2411 | | 2a | 7 | 127 | 21 |
| | | | 2b | 4 | 56 | 16 |
| ***Snow Grains*** | | | | | | |
| Sector Plate Clusters | 160 | | l | 49 | 831 | 196 |
| | | | w | 40 | 456 | 136 |
| Bullet Clusters | 67 | | 2a | 19 | 284 | 84 |
| | | | c | 55 | 959 | 243 |
| | | | n | 1 | 16 | 4 |
| Snow Grain Columns | 24 | | 2a | 35 | 201 | 94 |
| | | | c | 90 | 372 | 193 |

Table 2: Relative frequency of occurrence of the different ice crystal types from the South Pole 1992 photomicrographs, as well as the relative contributions to the total surface area and total volume. The values in bold type are the maximum values.

| Crystal Type | Relative Frequency (%) | Contribution to Total Surface Area (%) | Contribution to the Total Volume (%) |
|---|---|---|---|
| ***Diamond Dust*** | | | |
| Solid Columns | 10 | 15 | 7 |
| Plates | 9 | 12 | 9 |
| Pyramids | < 1 | < 1 | < 1 |
| Hollow Columns | < 1 | < 1 | < 1 |
| ***Blowing Snow*** | | | |
| Blowing Snow | **72** | **46** | 31 |
| Residual Blowing Snow | 8 | 6 | 5 |
| ***Snow Grains*** | | | |
| Sector Plate Clusters | <1 | 8 | 5 |
| Bullet Clusters | < 1 | 11 | **39** |
| Snow Grain Columns | < 1 | 1 | 3 |